BMC Chemistry

RESEARCH

Open Access

Expediting the bioactivity of zinc sulfide nanoparticles with copper oxide as a nanocomposite

S. Sharmila[1], A. Saranya[1*], M. Arulprakasajothi[2], R. Saranya[3], B. Srimanickam[4], Sunil Kumar Abel[1], Faiyaz Shakeel[5] and Md Faiyazuddin[6,7*]

Abstract

The regulatory role of zinc in bone formation extends to the activation of proteins associated with bone homeostasis. Furthermore, copper is well known for its antibacterial properties. This dual function underscores the significance of zinc and copper in maintaining a balance of bone structure and function. In light of the aforementioned, zinc sulphide/copper oxide nanocomposites were created in this instance using a straightforward coprecipitation technique. Copper oxide was used as a nanocomposite to improve the structural, morphological, and biological performance of zinc sulphide nanoparticles. The X-ray diffraction pattern confirmed a transformation in the crystal structure from cubic to rhombohedral, along with increase in intensity. Fourier transforms infrared analysis indicated the presence of functional groups. Scanning electron microscopy images demonstrated a morphological shift from non-uniform to distinct spherical nanoparticles, impacting the enhancement of material properties. The pathogenic activity of the zinc sulphide/copper oxide nanocomposites was tested against nine bacterial strains. In antimicrobial testing, zinc sulphide/copper oxide nanocomposites showed promising results, particularly against *Klebsiella pneumoniae* (zone of inhibition: 14 mm at 100 µg/mL compared to 7 mm by standard) and *Escherichia coli* (zone of inhibition: 11 mm at 100 µg/mL compared to 10 mm by standard) after 24 h with zone of inhibition matching or exceeding that of the standard (chloramphenicol). Zinc sulphide nanoparticles and zinc sulphide/copper oxide nanocomposites were evaluated for their antifungal activity against fungal stains from *Trichophyton rubrum, Aspergillus niger,* and *Aspergillus flavus*. After a 24-h period, it was discovered that zinc sulphide/copper oxide nanocomposites were effective against *Aspergillus flavus* (zone of inhibition: 19.4 mm at 100 µg/mL compared to 6.3 mm by standard) at all concentrations (25–100 mg/mL), with zones of inhibition identical to or greater than those of the standard (fluconazole). Certainly, based on these results, zinc sulphide/copper oxide nanocomposites could be promising materials for drug delivery.

Clinical trial registration: Not applicable.

Keywords Antibacterial, Antifungal, *Aspergillus flavus*, Copper oxide, *Klebsiella pneumonia*, Nanocomposite, Zinc sulfide

*Correspondence:
A. Saranya
saran.amrith@gmail.com
Md Faiyazuddin
md.faiyazuddin@gmail.com
Full list of author information is available at the end of the article

Introduction

Nanomedicine (or the use of materials with nanometer dimensions in medicine) has shown promise in treating osteomyelitis by delivering targeted therapies to infected bone tissue, prolonging drug delivery, avoiding immune system clearance, and reducing side effects [1]. Research in this area has explored the use of nanoparticles for improved drug delivery and imaging modalities for improved disease diagnosis and treatment monitoring [2]. Furthermore, the biogenic (or biological) synthesis of nanoparticles has enhanced antimicrobial properties and reduced the toxicity of such materials in the body [1, 2]. A class of nanomaterials known as nanocomposites (NCs) consist of two or more solid materials that have various physical and chemical characteristics. The distinctive catalytic, optical, and electrical characteristics of metal-based NCs can be tailored by modifying their size, shape, and surface. At the molecular level, they can be synthesized using inorganic or organic components to acquire new features.

A possible strategy for realizing broad functionality is the production of NCs. Blumstein reported the first study on NCs in 1961, and his subsequent investigations in 1965 showed even greater promise [1]. A NC can serve as a representative of synergistic properties that lacks in individual components. The high surface/volume ratio of NCs enables them to become materials for future applications. These findings also indicate new methods for eliminating the current constraints of microcomposites and monolithics. The overall characteristics of the end product can differ from and are more effective than those of the individual components. Batteries, gas sensing, prosthetic implants, and targeted drug delivery have all been improved from the use of NC materials compared to conventional materials [2].

As a consequence of their ability to accommodate biological functionalization, nanofeatures, etc., NCs are recognized for their use in the biomedical industry, such as for the treatment of infections and/or cancer cells [3, 4]. Additionally, they combat drug resistance and significantly reduce systemic toxicity. Despite the potent effects of the new generation of medications, the majority of them have drawbacks such as limited gastrointestinal permeability, poor stability, poor solubility in water, and resistance to bacteria and/or cancer cells [3]. It is important to explore sustainable alternatives and innovative approaches for therapeutic techniques to address environmental concerns and minimize impacts on future generations. Research on inorganic and polymeric carriers aims to identify materials with enhanced performance for various applications, including drug delivery and other therapeutic techniques. Advances in materials science can lead to more efficient and environmentally friendly solutions [4]. Modern society, industrialization, and innumerable human activities cause a variety of bacterial and viral ailments. In many scientific fields, including healthcare, manufacturing, food preservation, and water purification, the role of antibacterial agents is indispensable.

Osteomyelitis is a serious bone infection typically caused by pyogenic (pus-producing) bacteria, such as *Staphylococcus aureus* [5]. The infection can occur through bloodstream dissemination, direct bone contamination, or continuous spread from nearby tissues. Bacteria are indeed common causes of infection, but viruses, fungi, and parasites can also lead to various infections [5]. Osteomyelitis treatment is challenging due to antimicrobial resistance, antibiotic tolerance from metabolic changes or biofilm formation, limited antibiotic penetration into infected bone, and colonization of antibiotic-protected reservoirs within the bone substructure [5].

Compared with conventional antibiotics, NCs show promise for preventing existing resistance mechanisms, potentially reducing the likelihood of resistance development. The unique properties and mechanisms of action of these bacteria contribute to their potential effectiveness in addressing antibiotic resistance challenges [5, 6]. Researchers are currently particularly interested in producing NCs using different reducing and capping agents and evaluating how effective they are biologically in getting rid of bacteria and viruses [1, 2, 6]. Using this method, the precursors are allowed to dissolve in the selected solution, and under favourable thermodynamic conditions, the reaction produces simultaneous formation, growth, and coarsening. This approach's primary determinants of product morphology and size are the ripening, nucleation, and aggregation processes [6].

Since metals do not attach to a particular receptor on a bacterial cell, metal-based nanoparticles (NPs) function as nonspecific antibacterial agents. Additionally, metal-based NPs broaden the spectrum of their antibacterial activity and prevent germs from becoming resistant. The findings indicate that the first step toward nanotoxicity is electrostatic interactions between the cell surface and NPs, which are followed by an increase in the permeability of the membrane, morphological alterations in the cell, and their formation in the cytoplasm [5]. The use of semiconductor materials, especially metal chalcogenides, in photoluminescence, optoelectronics, solar cells, optical sensor devices, and other technologies has drawn attention because of the broadband gap [3, 4]. Zinc sulphide (ZnS) is a metal chalcogenide that has been studied and shown to be beneficial for a number of specific applications. It exhibits bandgaps of 3.68 and 3.77 eV and is found in the sphalerite cubic phase at normal temperature or the hexagonal wurtzite phase at a higher

temperature. It has typically been used in the optoelectronic industry because of its broadband bandgap [7–9]. There is a large surface-to-volume ratio in ZnS nanocrystals. Transition metals, including Ni, Mn, Cu, and Co, may be added in minuscule quantities to ZnS to adjust the band gap energy. This may result in better luminescence characteristics over a larger spectrum range as well as novel characteristics achieved by the dopants. In addition, the material has excellent thermal stability, strong chemical stability, low toxicity, high electronic mobility, and environmental safety.

The most common methods involved in the synthesis of metal NCs include the sol–gel method, spray pyrolysis, electrodeposition, vapor techniques, and so on [1]. Metal-doped ZnS was reported via different chemical methods by many researchers due to its excellent photocatalytic efficiency [10–23]. Sathishkumar et al. previously reported on ZnS nanocrystalline thin films doped with copper and aluminium using a sol–gel dip coating method [24]. When compared to other bacteria and concentrations, the resultant material demonstrated higher antibacterial activity against *Escherichia coli* because of the reduced crystallite size and strong surface-to-volume ratio of Cu doping (4%) in ZnS thin films. Similarly, Chaliha et al. produced Cu-doped ZnS NPs using a solvothermal method using mercaptosuccinic acid (MSA) and sodium citrate (SC) as capping agents [25]. When MSA was utilised as a capping agent, the particles demonstrated outstanding antibacterial activity against *Bacillus subtilis*. Many studies have concentrated on employing polymers or a reduced graphene oxide matrix to enhance ZnS properties. Researchers reported a nano-ZnS/polystyrene composite by using a surfactant-free emulsion polymerization method. By adjusting the reaction parameters, they tuned the morphology of the composite from that of a raspberry to that of a hollow sphere [26]. ZnS/polyaniline NCs prepared by the coprecipitation method acted as efficient electrocatalysts for oxygen evolution [27]. Using a hydrothermal approach, a ZnS-reduced graphene oxide (ZnS/rGO) NC has also been reported [28]. The prepared NC also functioned as a superior photocatalyst for synthesizing benzazoles. By photocatalytically degrading methyl orange in an aqueous solution, the photocatalytic activity of ZnS/rGO NCs produced using a single-step solvothermal technique were examined [29]. Furthermore, the surface reaction rate constant of the ZnS/rGO NCs was six times greater than that of the ZnS NPs, indicating that the NCs exhibited more photocatalytic activity than the former. Dadi et al. investigated the antibacterial properties of zinc oxide (ZnO) and copper oxide (CuO) NPs produced via the sol–gel method [30].

Experiments against *Staphylococcus aureus, Escherichia coli*, and *Pseudomonas aeruginosa* were conducted using the disc and well diffusion method [29]. During the terminal stationary phase, the ZnO NPs lose activity, while the CuO NPs maintain this activity. To create CuO NPs, Khatoon et al. employed a chemical reduction technique involving oxalic acid, sodium borohydride, and trisodium citrate as different chelating and reducing agents [31]. Among other agents, sodium borohydride-assisted CuO exhibits greater bacterial activity against a range of pathogens. As one of the simplest, economical, and quick processes, coprecipitation offers perfect stoichiometry control, low-temperature synthesis, and good chemical uniformity and can be readily applied on a wider scale for commercial applications. It produces an extremely pure nanomaterial in a way that is safe for the environment and does not require the use of hazardous chemical solvents or high-pressure or temperature treatments [32]. Several metal oxide-based NCs have been investigated for dye removal/degradation, photocatalytic properties, antioxidant potential, and antibacterial activity [33–39]. ZnO and CuO-based nanomaterials have also been investigated for dye removal/degradation in the literature [40–42]. Many studies have been conducted on Cu/ZnS, but they have all been aimed at improving the luminescence and catalytic activity of various dyes [9, 19–23]. Various ZnO and CuO/CuS-based NCs have also been studied for their antibacterial activity and adsorption potential [43–46]. However, the information regarding the antibacterial and antifungal potential of ZnS/CuO@NCs is scarce in the literature. As a result, the objective of the present study was to determine the potential of enhancing the bioactivity (antibacterial and antifungal) of ZnS/CuO@NCs for osteomyelitis therapy. The ZnS/CuO@NCs used in this work were synthesized using a low-cost, one-pot coprecipitation technique, and their antibacterial, antifungal, optical, and structural properties were assessed. Chemical coprecipitation is one of the best options for synthesizing ZnS NPs since it has several benefits, including excellent purity and a uniform chemical structure [14, 22]. Furthermore, coprecipitating ZnS is a preferable option for synthesizing the material since it reduces the possibility of turning ZnS into ZnO even at higher temperatures during calcination. They can provide controlled drug release, improving the effectiveness of antibiotics at the infection site while minimizing systemic side effects. Additionally, NCs may offer enhanced mechanical properties for bone regeneration in osteomyelitis-affected areas.

Materials and methods

Chemicals and reagents

Himedia (Mumbai, India) provided the analytical grade ethanol, copper acetate ($Cu(CH_3COO)_2$), sodium sulphide nonahydrate ($Na_2S{\cdot}9H_2O$), and zinc acetate

dihydrate ($Zn(CH_3CO_2)_2{\cdot}2H_2O$). Chloramphenicol (CMP; 50 mg/L) and fluconazole (FCZ; 5000 mg/L) were obtained from Sigma Aldrich (Mumbai, India) and sued as antibacterial and antifungal standard, respectively. Double distilled water (DDW) was employed throughout the experiment for dilituion purpose. Semisolid Mueller–Hinton agar (MHA) was purchased from SD Fine Chemicals (Mumbai, India). The detail information regarding each material is presented in Table 1. Abbes Biotech (Coimbatore, India) provided the bacterial strains of *E. coli, K. pneumoniae, S. dysenteriae, P. vulgaris, P. aeruginosa, S. aureus, S. pneumoniae,* and *B. subtilis*, while K.G. Hospital (Coimbatore, India) provided the fungal strains.

The purity was provided by supplier of each material.

Synthesis of ZnS and ZnS/CuO nanocomposites

After adding $Zn(CH_3CO_2)_2{\cdot}2H_2O$ (0.2 M) to 100 mL of DDW at room temperature, the mixture was continuously agitated for 30 min using a mechanical stirrer. $Zn(CH_3CO_2)_2{\cdot}2H_2O$ was aggressively agitated and allowed to completely dissolve in DDW, forming a transparent, homogenous solution. The zinc precursor solution was added dropwise to an equimolar $Na_2S.9H_2O$ solution that had been prepared independently. When the $Na_2S.9H_2O$ solution was completely mixed, a milky mixture developed, indicating the start of the ZnS NPs production. For two hours, the resultant liquid was continuously churned. By centrifuging the solution at 3000 rpm, a white precipitate appeared was removed followed the removal of residual salts using DDW and ethanol. After washing, the precipitate was recovered and dried at 80 °C. In the same way, 0.4 M and 0.6 M ZnS NPs were prepared [27]. The formation of ZnS NPs is exhibited in Scheme 1. To prepare ZnS/CuO@NCs, 100 mL of a 0.1 M $Cu(CH_3COO)_2$ solution was added dropwise to a 0.5 M ZnS solution under continuous stirring for 2 h at room temperature. To eliminate any residual material present in the mixture, the retrieved precipitate was centrifuged initially with DDW and then with ethanol. The samples were subsequently dried in an oven at 80 °C and utilized for further characterization. Each synthesis was performed in triplicates. The yield (% w/w) of ZnS NPs and ZnS/CuO@NCs was determined to be 84.12 ± 1.54 and 86.32 ± 1.64% w/w, respectively.

Characterization

X-ray diffraction (XRD)

XRD is a widely acknowledged non-destructive method that yields detailed information about the chemical composition and crystal structure of many substances. An X'Pert PRO BRUKER diffractometer equipped with CuKα radiation (λ = 1.5406 Å) was used to analyze the structural phase and crystallinity of the resultant nanocomposite at an angle (2θ) ranging from 10 to 80°.

Fourier transform infrared (FTIR) spectroscopy

To investigate the presence of vibrations between 4000 and 400 cm^{-1}, the prepared materials were exposed to a FTIR utilizing a Bruker Alpha II spectroscope.

Scanning electron microscopy (SEM) and energy dispersive X-ray (EDX) analyses

The surface morphology of the synthesized nanocomposites was investigated using a SEM (SEM; JEOL JSM 6390, Tokyo, Japan). The presence of different elements in the NP sample was determined by EDX analysis in conjunction with SEM. ZAF correction was applied during EDX programming to resolve the specimen, where Z indicates the atomic number, A represents the absorbance, and F indicates fluorescence. To obtain the final elemental characterization results for the sample, data were extracted from the perfectly formed particles exposed on the top of the plate.

Antibacterial activity

Following guidelines from the Clinical Laboratory Standards Institute (CLSI), the antibacterial performance of ZnS NPs and ZnS/CuO@NCs was investigated using the well diffusion method against eight different organisms at different concentrations (25, 50, 75, and 100 µg/

Table 1 The information regarding the materials used

Compound	Molecular formula	Grade	Purity (%)	Source
Copper acetate	$Cu(CH_3COO)_2$	Analytical	98.5	Himedia
Sodium sulphide	$Na_2S.9H_2O$	Analytical	99.1	Himedia
Zinc acetate	$Zn(CH_3CO_2)_2{\cdot}2H_2O$	Analytical	98.6	Himedia
Chloramphenicol	$C_{11}H_{12}ClN_2O_5$	Pharmaceutical	98.0	Sigma Aldrich
Fluconazole	$C_{13}H_{12}F_2N_6O$	Pharmaceutical	98.0	Sigma Aldrich
Ethanol	C_2H_5OH	Analytical	99.8	Himedia
Water	H_2O	Double distilled	–	Distillation unit

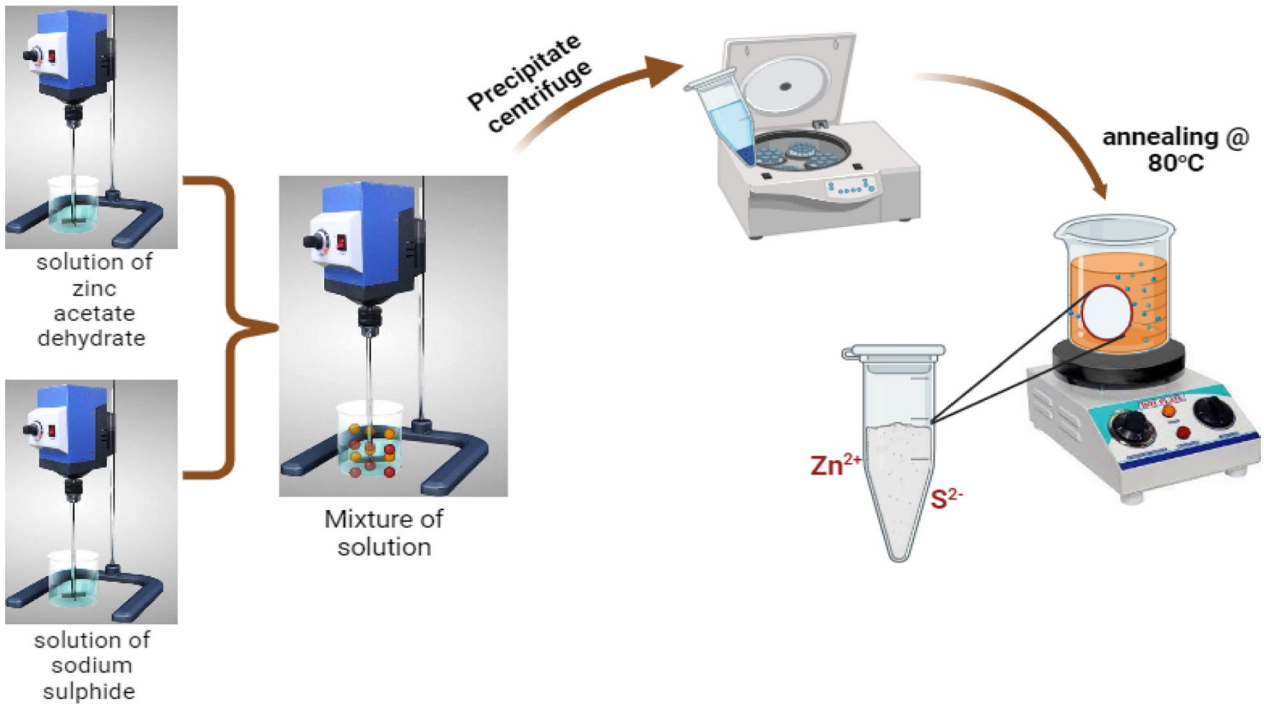

Scheme 1 Scheme for the synthesis of ZnS NPs using a simple coprecipitation approach

mL): *E. coli, K. pneumoniae, S. dysenteriae, P. vulgaris, P. aeruginosa, S. aureus, S. pneumoniae,* and *B. subtilis* [47]. In summary, 20 mL of semisolid MHA were added to Petri dishes. Before being cultured with 1.5×10^6 CFU/mL suspensions of each bacteria separately on the surface of the solid medium MHA using a sterile brush, the bacteria were cultivated in nutrient broth (NB) for 24 h. On the surface of the inoculated agar plates, NPs at different concentrations (ranging from 25 to 100 µg/mL) were impregnated into the wells (6 mm in diameter). The plates were incubated at 37 °C for 24 h. The antibacterial activity was ascertained by measuring the diameter of the inhibitory zone (mm). The diameter of zone of inhibition was measured using a metric ruler. CMP was used as a positive control.

Antifungal activity

The effectiveness of the synthesized ZnS NPs and ZnS/CuS@NCs was assessed against three different fungal strains, i.e., *T. rubrum, A. niger*, and *A. flavus.* Three types of fungal strains were segregated on agar with potato dextrose. The turbidity of the well after 24 h at 30 °C was used to compute the minimum inhibitory concentration [45]. Following a 24-h incubation period, the cultivated fungus was swabbed onto potato dextrose agar plates using cotton-tipped swabs. The standard drug used was FCZ. Phosphate buffer saline was used to prepare the samples at various concentrations (25, 50, 75, and 100 µg/mL) via the well diffusion method and well puncture. Approximately 20 µL of the appropriate sample concentration was added to each well. The samples were incubated at room temperature for 24 h.

Statistical analysis

One-way analysis of variance (ANOVA) followed by Dunnett's test was used for the statistical analysis, with a P value of 0.05 considered significant. Graph-Pad Prism Software (San Diego, CA, USA) was utilized for all data analysis, and the tests were run three times.

Results and discussion

XRD

Figure 1 shows the structural information, such as the phase purity, crystalline nature, and structure of the ZnS NPs and ZnS/CuO@NCs. Three noticeable broad peaks that corresponded to the (1 1 1), (2 2 0), and (3 1 1) reflection planes were seen in the XRD pattern of ZnS (0.2, 0.4, and 0.6 M) for all three samples. The produced powder's diffraction peak positions all match the cubical zinc mixed structure and are in good agreement with the results presented in JCPDS No. 05–0566 [23–25, 48]. Peak broadening signifies the NPs' creation. A small variation was seen with different ZnS concentrations (0.2, 0.4, and 0.6 M), as Fig. 1 illustrates. The results showed that 0.6 M was optimized to attain a better intensity, and the NCs were prepared using the same concentration. The

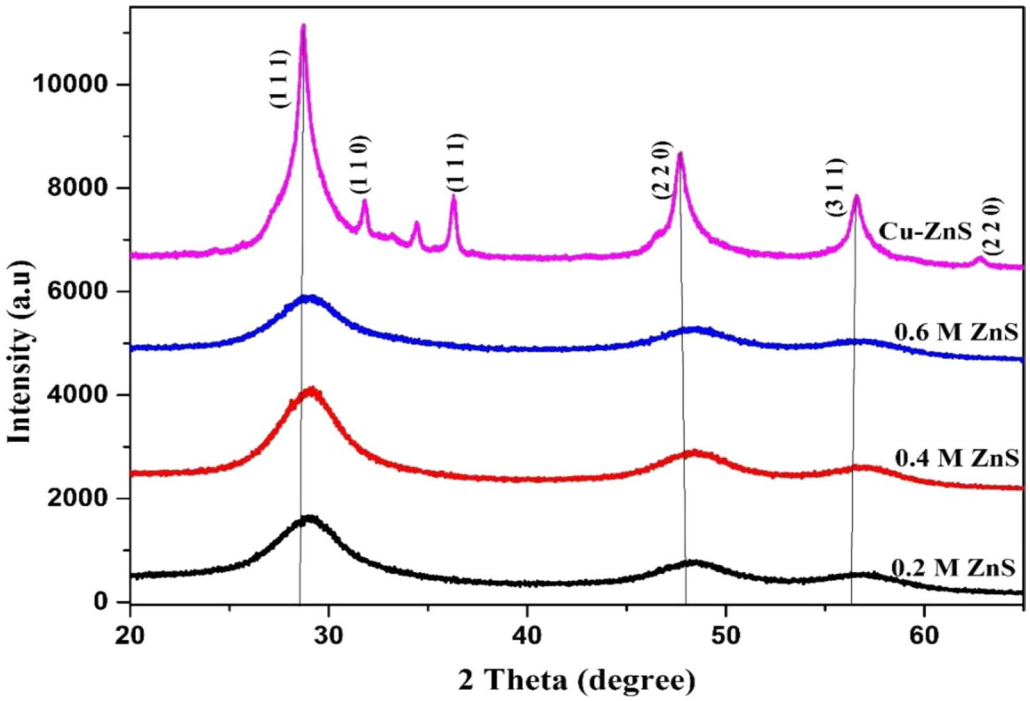

Fig. 1 XRD patterns of **a** ZnS NPs and **b** ZnS/CuO@NCs to identify crystallinity of prepared materials

XRD pattern of ZnS/CuO in Fig. 1 displays extra peaks at 32.63°, 36.54°, and 61.57°, which correspond to the (110), (111), and (220) planes, respectively. These peaks suggest that the ZnS/CuO@NCs display the following peaks, which correspond to ZnS: (1 1 1), (2 2 0), and (3 1 1), as well as additional metallic peaks from CuO. On the other hand, the structural deformation (monoclinic) that occurs due to the formation of the NC and the crystalline nature of the material also increase upon the addition of CuO without any further impurities. Using the Debye-Scherer formula, the average crystallite size of the nanomaterials was calculated as follows:

$$D = \frac{K\lambda}{\beta cos\theta} \tag{1}$$

where D is the crystalline size, K indicates Scherrer's constant (0.98), λ denotes the wavelength (1.54 Å), and β represents the full width at half maximum. Using the following equations, the dislocation density and microstrain were estimated and are shown in Table 2.

$$\delta = \frac{1}{D^2} \tag{2}$$

$$\varepsilon = \frac{\beta cos\theta}{4} \tag{3}$$

Table 2 XRD parameters of ZnS NPs and ZnS/CuO@NCs at different concentrations

Concentration (M)	Crystallite size (nm)	Dislocation density ($\times 10^{14}$ lines/m^2)	Strain ($\times 10^{-3}$ lines^{2}m^{-4})
0.2	37.80	6.998	9.5747
0.4	59.35	2.838	6.0997
0.6	61.10	2.675	5.9247
ZnS:CuO	11.36	77.48	32.67

Table 2 indicates that as molarity increased, grain size increased while strain and dislocation density dropped. The development of a NC led to a considerable reduction in the size of the crystallite. Alharbi et al. found similar results for a ZnS/chitosan composite utilizing the hydrothermal method, observing that the average crystallite size was 11.50 nm [49]. A ZnS-silver sulphide NC made by Srivastava et al. using the precipitation method had larger crystallites than the crystals found in the present work [48].

FTIR

Figure 2a, b shows the FTIR transmittance spectra of ZnS and ZnS/CuO@NCs. The transmittance peaks for ZnS were found at 612, 668, 1020, 1341, 1428, 1559, 2103, and 3301 cm^{-1}, as per the FTIR spectrum analysis. The Zn–S stretching vibration mode and the cubic

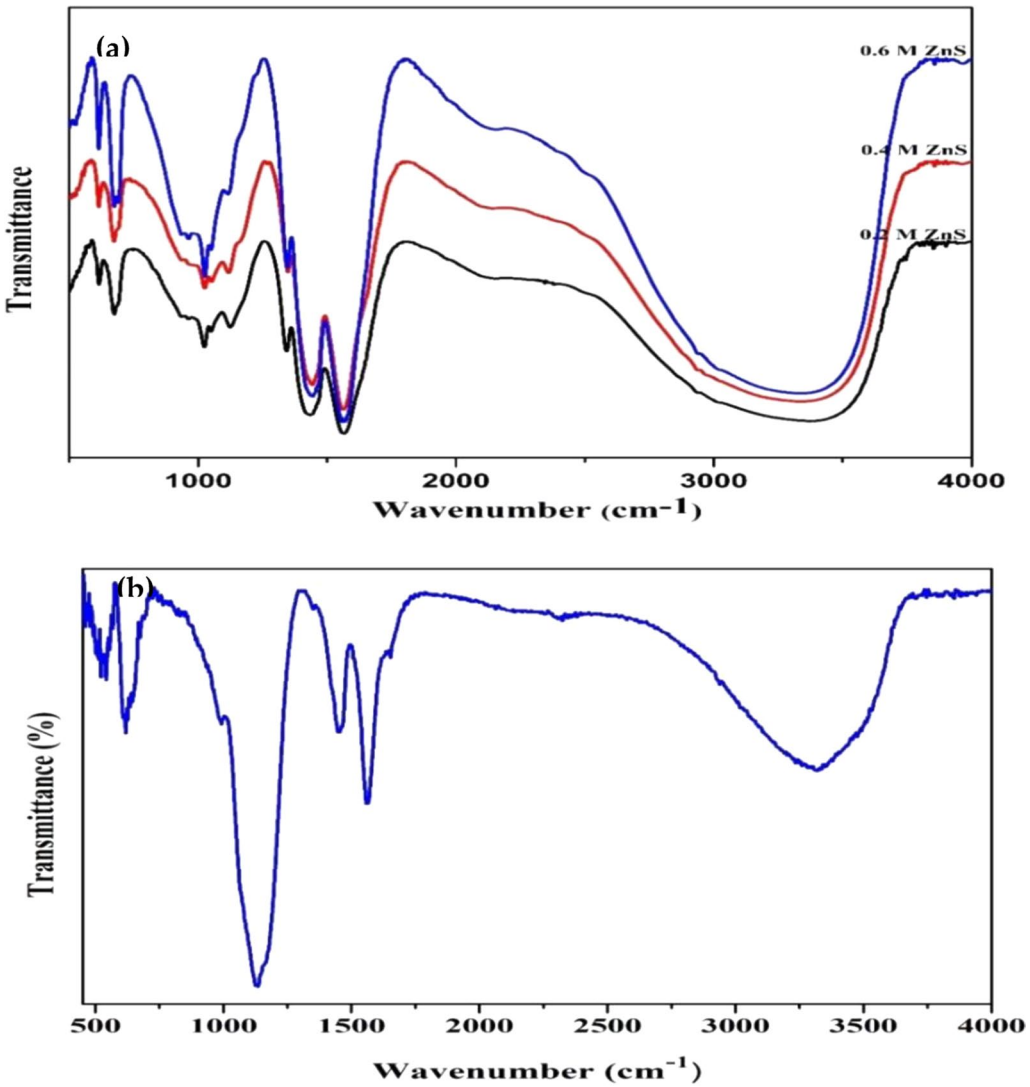

Fig. 2 FTIR spectra of **a** ZnS NPs and **b** ZnS/CuO@NCs to identify the crystallinity and different functional groups of prepared materials

Zn–S features are associated with the peaks at 612 and 668 cm^{-1}, respectively [50–52]. Organic molecules have a vibrational mode, and their presence was established by the discovery of a peak at 1020 cm^{-1} [51]. The peak at 1428 and 1559 cm^{-1} was caused by symmetric stretching modes in the carboxylic group of the precursor (zinc acetate) and –C=O on the surface of the generated NPs during the spectrum recording process [52]. The strong and broad transmittance peak that is observed for all ZnS NPs between 3410 and 3465 cm^{-1} is consistent with the O–H stretching and bending modes of H_2O [53]. The transmittance peak moved from 612 cm^{-1} to 522 cm^{-1} as a result of the Cu–O vibration mode (Fig. 2b). Further, the addition of copper acetate suppressed the ZnS peak found at 668 and 1020 cm^{-1}, and the presence of CuO in ZnS was indicated by a sharp peak at 1133 cm^{-1}. Additionally, the broad transmittance peak caused by the O–H molecule shrank.

SEM and EDX analysis

Surface respite, grain formation, and the effects of the addition of the composites were all examined by SEM. Figure 3a–d displays SEM images of ZnS/CuO@NCs and 0.2 M, 0.4 M, and 0.6 M ZnS NPs that were annealed at 80 °C. The results obtained from 0.2 and 0.4 M ZnS NPs exhibited nonuniform surface morphologies with agglomeration due to the experimental conditions, including temperature, pH, precursor composition, reaction time, etc. By further increasing

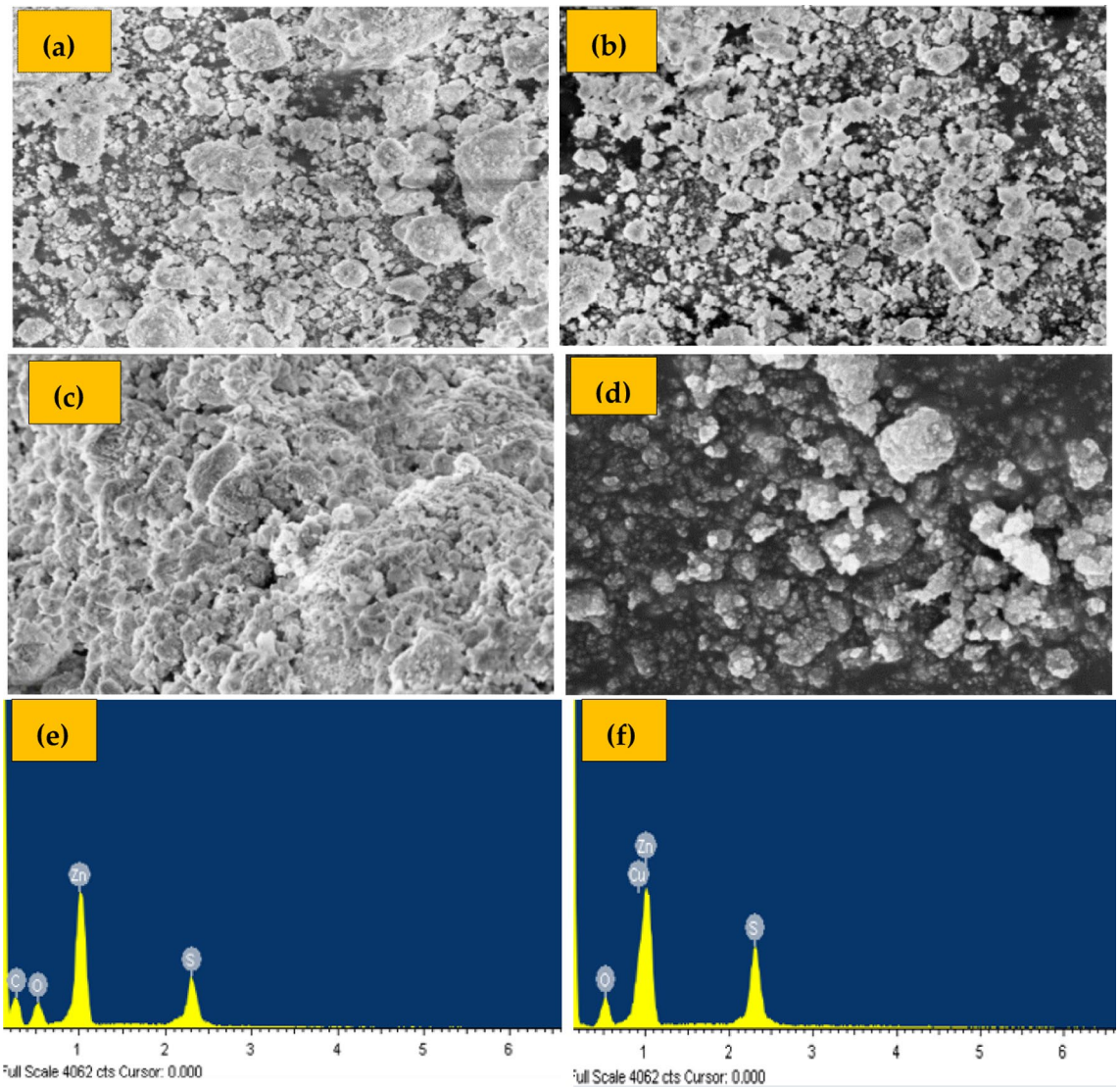

Fig. 3 SEM images of **a** 0.2 M, **b** 0.4 M, **c** 0.6 M ZnS NPs and **d** ZnS/CuO@NCs to identify the size and shape of prepared materials. EDX spectra of **e** 0.6 M ZnS NPs and **f** ZnS/CuO@NCs to identify the elemental distribution in prepared materials

the molar concentration to 0.6 M, the accumulation of small spherical particles occurred (Fig. 3c) [54, 55]. The ZnS/CuO@NCs exhibited smooth surface spherical particles, as illustrated in Fig. 3d. These results imply that the shape and size of ZnS are influenced by CuO and molar concentration. This confirmed the excellent sedimentation and well-dispersed nature of the synthesized ZnS/CuO@NCs. The purity and composition of the produced materials were determined from the EDX spectrum, as shown in Fig. 3e, f. The spectrum shows the distributions of Zn, S, Cu, and O relative to their stoichiometric ratios without the presence of any other extra compounds, according to the obtained results.

Antibacterial activity

Against various gram-positive and gram-negative bacteria, the antibacterial efficacy of ZnS NPs and ZnS/CuO@NCs was assessed at varying concentrations (25, 50, 75, and 100 µg/mL) over a 24-h period. The antibacterial activity of different samples was statistically compared using one-way ANOVA followed by Dunnett's test. The antibacterial activity of the produced materials against *E. coli, S. dysenteriae, B. subtilis, P. aeruginosa, P. vulgaris, K. pneumoniae,* and *S. aureus* is displayed in Fig. 4. It was concluded that with an increase in concentration, a zone of inhibition was sufficient for most of the bacteria. ZnS NPs exhibited a better response against *S. aureus* than against other

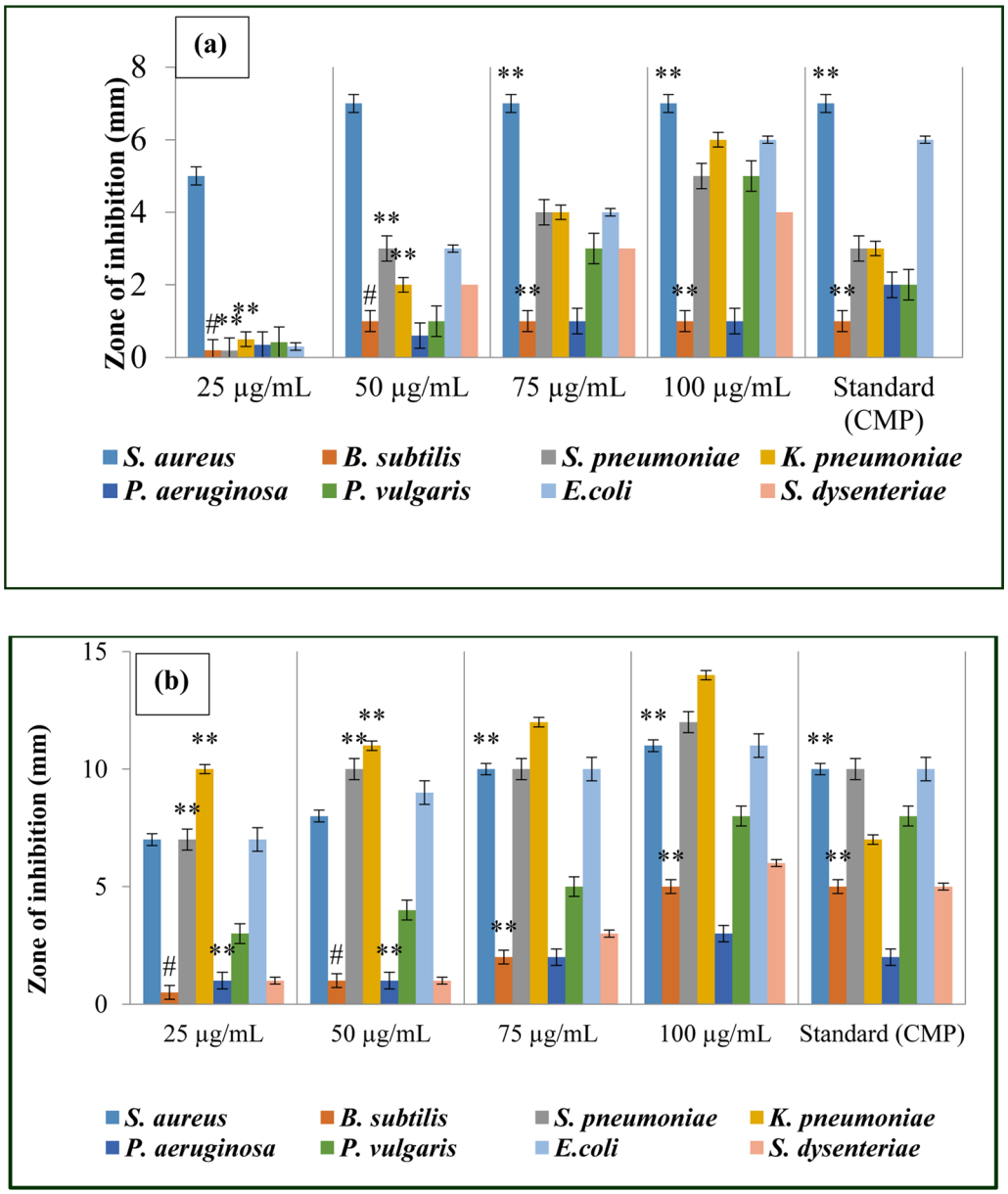

Fig. 4 Antibacterial effects of **a** 0.6 M ZnS NPs and **b** ZnS/CuO@NCs over various gram positive and gram-negative pathogen in comparison to standard CMP. $^{\#}p < 0.01$, $^{*,**}p = 0.05$-comparison using ANOVA and Dunnett's method

microorganisms; when 0.1 M CuO was introduced, the NCs produced good results for *K. pneumoniae,* followed by *E. coli* ($^{\#}p < 0.01$, $^{*,**}p = 0.05$-comparison using ANOVA and Dunnett's method). Gram-positive bacteria are surrounded by a thick layer of peptidoglycan, while it is absent in gram-negative bacteria. However, two thin layers—an exterior layer called lipopolysaccharide and an interior layer called peptidoglycan—protect gram-negative bacteria. Gram-negative bacteria's vulnerability to NCs may be influenced by the negative charge of lipopolysaccharide molecules. The majority of NPs produce positive ions (Zn^{+}), which these negatively charged molecules have a larger affinity for. This enhances ion uptake and causes intracellular damage [56]. The antibacterial efficiency of NPs is often influenced by a variety of parameters, including size, surface area, polarity, and shape. Furthermore, the electrostatic interaction between positively charged NPs and negatively charged bacterial cells is essential for the efficiency of NPs as bactericidal materials.

Reactive oxygen species (ROS) are produced as a result of this interaction, which inhibits bacterial growth and causes cell death [57–59]. Since 0.6 M ZnS exhibits good structure and morphology, this composition was utilized to examine the biological performance of the materials. Except for *S. aureus,* the ZnS NPs had no inhibitory effect at concentrations less than 25 µg/mL. Almost all bacteria displayed the least zone of inhibition upon the addition of CuO at 50 µg/mL and above. ZnS produces ROS, including superoxide anions (O–), hydroxyl ions (OH–), and hydroxyl radicals (OH) [57]. Furthermore, Cu^{2+} ions bind to protein reactive groups such as carboxyl (–COOH), imidazole ($C_3H_4N_2$), thiol (R-SH), and amino ($–NH_2$) groups. This disrupts cell activity and eventually results in bacterial mortality. The antibacterial effects of prepared CuO/ZnS@NCs against various bacterial strains were also compared to the similar nanomaterials reported in the literature and results are presented in Table 3. The zone of inhibitions for ZnO/CuO@NC against *E. coli*, *K. pneumoniae*, *P. auruginosa*, and *S. aurius* have been repoerted to be 24.00, 0.00, 13.00, and 18.50 mm, respectively [43]. The zone of inhibitions for ZnO/CuO@NC against *E. coli*, *K. pneumoniae*, *P. auruginosa*, and *S. aurius* have been repoerted to be 12.83, 9.11, 12.17, and 18.00 mm, respectively by another research [46]. The zone of inhibitions for ZnS thin films against *E. coli*, *B. subtilis*, *P. auruginosa*, and *S. aurius* have been repoerted to be 11.00, 11.00, 12.00, and 13.00 mm, respectively [24]. The antibacterial results of present ZnO/CuO@NC showed the significant antibacterial activity against *K. pneumoniae* compared to those reported in the literature [43, 46]. However, the antibacterial effects of present ZnO/CuO@NC were inferior to those reported for other bacterial strains [43, 46]. Overall, the results obtained in the present study are in line with previous reports by Dwivedi et al. [59] and Sathishkumar et al. [24]. CuO/ZnS@NC exhibited potent antibacterial effects against *K. pneumoniae* compared to other pathogens and the positive control. Zinc ions (Zn^{2+}) released from ZnS NPs can exhibit osteogenic properties, as zinc plays a crucial role in enzyme catalysis and activation reactions important for bone health [59–61]. Furthermore, Zn^{2+} can promote bone growth by accelerating apatite nuclei to fasten mineralization [61].

Table 3 Comparison of antibacterial activity (zone of inhibition) of ZnS/CuO@NCs with similar materials reported in the literature

Material	Bacterial strain	Zone of inhibition (mm)	Refs.
ZnO/CuO@NC	*E. coli*	24.00	[43]
	K. pneumoniae	0.00	
	P. aeruginosa	13.00	
	S. aurius	18.50	
ZnS films	*E. coli*	11.00	[24]
	B. subtilis	11.00	
	P. aeruginosa	12.00	
	S. aurius	13.00	
ZnO/CuO@NC	*E. coli*	12.83	[46]
	K. pneumoniae	9.11	
	P. aeruginosa	12.17	
	S. aurius	18.00	
ZnS/CuO@NC	*E. coli*	11.00	Present work
	K. pneumoniae	14.00	
	P. aeruginosa	3.00	
	S. aurius	11.00	
	B. subtilis	5.00	

Antifungal activity

T. rubrum, A. niger, and *A. flavus* were among the species against which the antifungal efficacy of ZnS NPs and ZnS/CuO@NCs was investigated at minimum inhibitory concentration of 0.6 M during a 24-h period at doses of 25, 50, 75, and 100 µg/mL as compared with standard FCZ. The antifungal activity of different samples was statistically compared using one-way ANOVA followed by Dunnett's test. The results of antifungal activity are shown in Fig. 5. Antifungal results reveal that ZnS/CuO@NCs can kill gram-negative bacteria ($\#p < 0.01$, $*,**p = 0.02$ comparison using ANOVA and Dunnett's method) more efficiently by adhering to nucleic acids and connecting to functional domains of crucial proteins because their protective barrier is thinner and because they have a lipopolysaccharide layer surrounding their membrane [59]. ZnS NPs showed better activity against *T. rubrum* at all concentrations than did the NCs; however, the ZnS NPs did not show any activity against *A. niger* or *A. flavus* at 25 mg/mL. Both the NPs and NCs exhibited better inhibition of *A. flavus* at all concentrations (50, 75, and 100 mg/mL) than did the other fungi. The biological performance of the composite, ZnS/CuO@NCs, increased with increasing concentration compared with that of the ZnS NPs, which may be due to its cell structure. The standard (FCZ) did not inhibit *A. flavus*. The addition of CuO to ZnS composites produced the strongest antibacterial effect since it released copper ions, which are highly reactive and have significant bactericidal effects [59]. The synergistic effects of ZnS NPs with CuO as NCs in antibacterial and osteogenic applications hold promise. Investigating the specific underlying mechanisms and optimizing the composition will contribute to advancing these beneficial effects in practical applications. The potential of ZnS NPs to promote

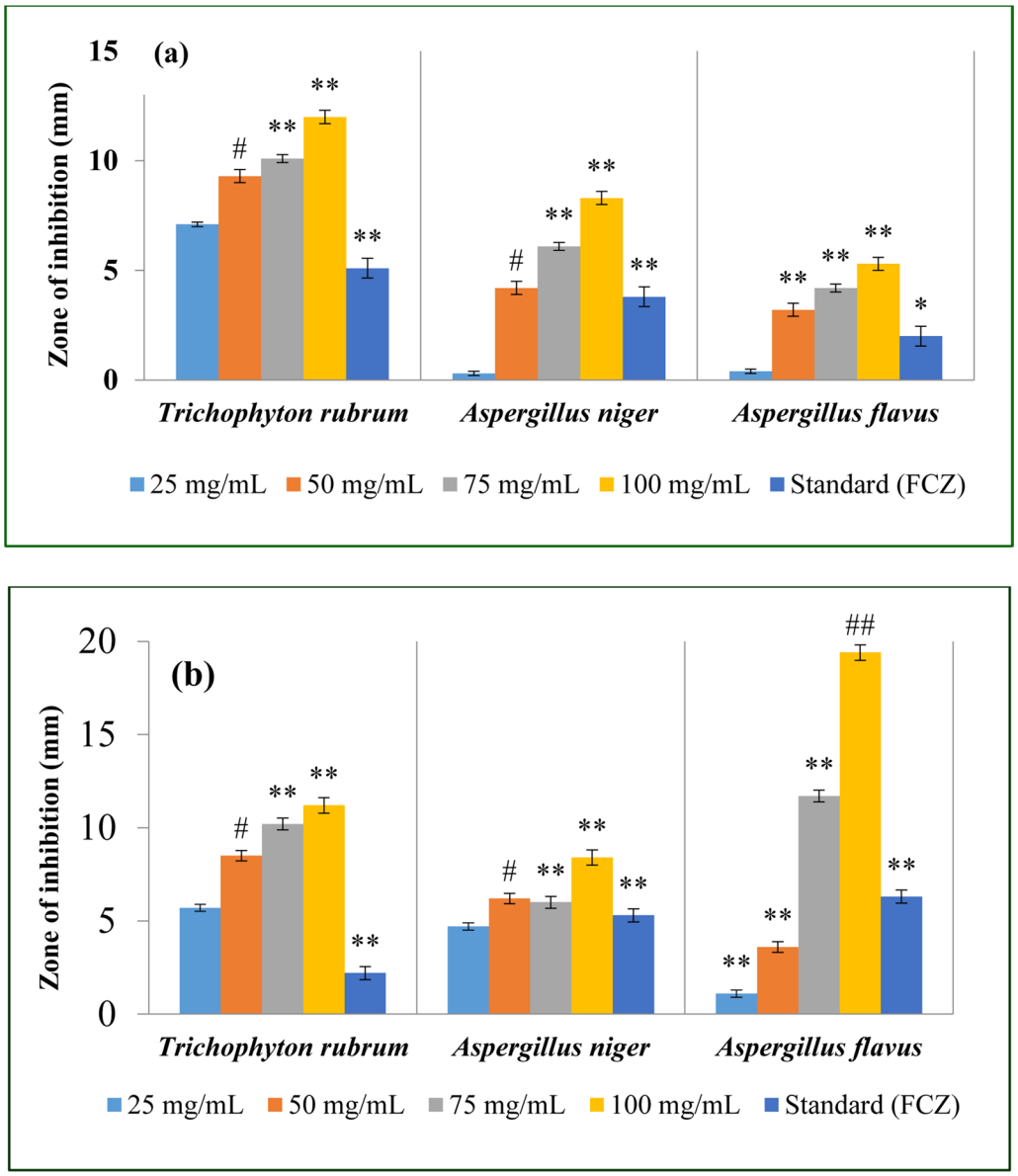

Fig. 5 Antifungal effects of **a** 0.6 M ZnS NPs and **b** ZnS/CuO@NCs against *T. rubrum, A. niger* and *A. flavus* at 25, 50, 75, 100 mg/mL, and FCZ (standard. $^{\#}p < 0.01$, $^{*,**}p = 0.02$ comparison using ANOVA and Dunnett's method)

cartilage formation and influence bone homeostasis could lead to significant advancements in regenerative medicine and orthopedic treatments, opening new avenues for therapeutic strategies.

Limitation of the study and potential areas for future work

In the present study, both ZnS NPs and ZnS/CuO@NCs were successfully synthesized, characterized, and evaluated for their antibacterial and antifungal activities. However, the main limitation of the study is that all evaluations were performed at in vitro models. As a result, there are several potential areas such as stability studies, in vivo pharmacodynamics studies, pharmacokinetics studies, toxicity studies, and clinical studies are still available for future work.

Conclusion

We effectively synthesized ZnS NPs and ZnS/CuO@NCs using a simple coprecipitation approach. Their biological performance was assessed, and 0.6 M ZnS NPs and ZnS/CuO@NCs were found to be promising

in all the studies. FTIR analysis verified the presence of various functional groups in the NPs as well as in the NCs. ZnS NPs had a nonuniform shape at 0.2 and 0.4 M, which changed to spherical-like particles at 0.6 M according to the SEM analysis. However, the NC had a transparent, smooth surface with spherical particles. The efficiency of ZnS against bacteria increased when it was prepared as a composite, and high inhibition was obtained for *K. pneumoniae* at all concentrations (25–100 µg/mL) after 24 h. Additionally, the ZnS/CuO@NCs performed better against *A. flavus* as antifungal agents after 24 h. Exploring the preparation methods, mechanisms, influencing factors, and recent research progress on the antifungal and antibacterial properties of ZnS/CuO@NCs provides a holistic view of their potential applications and safety considerations, especially for osteomyelitis, where Zn has been commonly used. The use of ZnS/CuO@NCs in regenerative medicine holds promise for enhancing cartilage formation and impacting bone homeostasis, potentially revolutionizing orthopedic treatments and paving the way for innovative therapeutic approaches. While, there are indications of positive effects on bone-related cells, additional research in terms of characterization, stability, preclinical, and clinical studies is needed to conclusively determine the impact of these agents on osteomyelitis and overall efficacy in musculoskeletal applications. As the prepared NCs revealed superior biological performance compared with previous findings, the osteosarcoma performance of the material will be examined in the future. After the collection of preclinical and clinical data, the prepared material could be explored for biomedical applications in the treatment of osteomyelitis and musculoskeletal disorders.

Acknowledgements
Authors are thankful to the Researchers Support Project number (RSPD2024R1040), King Saud University, Riyadh, Saudi Arabia for supporting this work. Sharmila S and Saranya A expresses her gratitude to Vel Tech Rangarajan Dr. Sagunthala R&D Institute of Science and Technology, Chennai, for providing the essential research facilities required for this study. Md. Faiyazuddin appreciates the support from Al-Karim University in research affairs.

Author contributions
SS: conceptualization, methodology, investigation, data curation, writing—original draft; AS: conceptualization, supervision, project administration, validation, writing review and editing; MA: methodology, investigation, data curation, RS: formal analysis, data curation, software; BS: software, validation, data curation; SKA: methodology, data curation, formal analysis; FS: funding acquisition, data curation, resources, visualization, validation, writing—review and editing; MF: conceptualization, supervision, project administration, writing review and editing.

Funding
"This work was funded by the Researchers Supporting Project number (RSPD2024R1040), King Saud University, Riyadh, Saudi Arabia".

Data availability
No datasets were generated or analysed during the current study.

Declarations

Ethics approval and consent to participate
Not applicable.

Consent for publication
Not applicable.

Competing interests
The authors declare no competing interests.

Author details
[1]Department of Physics, Centre for Thermal Management, Vel Tech Rangarajan Dr Sagunthala R&D Institute of Science and Technology, Chennai, Tamil Nadu 600062, India. [2]Department of Mechanical Engineering, KCG College of Technology, Chennai, Tamil Nadu 600097, India. [3]Department of Biotechnology, Nehru Arts and Science College, Coimbatore, Tamil Nadu, India. [4]Centre for Sustainable Energy, Department of Mechanical Engineering, Jaya Engineering College, Thirunindravur, Chennai, Tamil Nadu 602024, India. [5]Department of Pharmaceutics, College of Pharmacy, King Saud University, 11451 Riyadh, Saudi Arabia. [6]School of Pharmacy, Al-Karim University, Katihar, Bihar 854106, India. [7]Centre for Global Health Research, Saveetha Institute of Medical and Technical Sciences, Chennai, Tamil Nadu 600077, India.

Received: 27 August 2024 Accepted: 9 October 2024
Published online: 19 October 2024

References

1. Omanović-Mikličanin E, Badnjević A, Kazlagić A, Hajlovac M. Nanocomposites: a brief review. Health Tech. 2020;10:51–9.
2. Malhotra BD, Ali MA. Nanomaterials for biosensors: Fundamentals and applications. In: Malhotra BD, Ali MA, editors. Micro and nano technologies. Berlin: Springer; 2018. p. 145–59.
3. Wang C, Li J, Amatore C, Chen Y, Jiang H, Wang XM. Gold nanoclusters and graphene nanocomposites for drug delivery and imaging of cancer cells. Angew Chem Int Ed. 2011;50:11644–8.
4. Kubacka A, Diez M, Rojo D, Bargiela R, Ciordia S, Zapico I, et al. Understanding the antimicrobial mechanism of TiO_2-based nanocomposite films in a pathogenic bacterium. Sci Rep. 2014;4:E4134.
5. Saidykhan L, Abu Bakar MZB, Rukayadi Y, Kura AU, Latifah SY. Development of nanoantibiotic delivery system using cockle shell-derived aragonite nanoparticles for treatment of osteomyelitis. Int J Nanomed. 2016;11:661–73.
6. Emrooz HBM, Heidari MA, Nazarpour S, Karimi H. Compulsory co-precipitation", a novel and rational route for the synthesis of nanomaterials; mesoporous zinc sulfide is the first case. J Alloys Compd. 2021;860:E157928.
7. Kalyane D, Raval N, Maheshwari R, Tambe V, Kalia K, Tekade RK. Employment of enhanced permeability and retention effect (EPR): Nanoparticle-based precision tools for targeting of therapeutic and diagnostic agent in cancer. Mater Sci Eng C. 2019;98:1252–76.
8. Ajibade PA, Oluwalana AE, Sikakane BM, Singh M. Structural, photocatalytic and anticancer studies of hexadecylamine capped ZnS nanoparticles. Chem Phys Lett. 2020;755:E1378113.
9. Murugadoss G. Luminescence properties of co-doped ZnS:Ni, Mn and ZnS:Cu, Cd nanoparticles. J Lumin. 2012;132:2043–8.
10. Chitkara M, Singh K, Sandhu IS, Bhatti HS. Photo-catalytic activity of Zn1−xMnxS nanocrystals synthesized by wet chemical technique. Nanoscale Res Lett. 2011;6:E438.
11. Song L, Hu J, Lu X, Lu Z, Xie J, Hao A, Cao Y. Boosting the photocatalytic activity and resistance of photostability of ZnS nanoparticles. Inorg Chem. 2022;61:8217–25.
12. Yu D, Fang H, Qiu P, Meng F, Liu H, Wang S, et al. Improving the performance of ZnS photocatalyst in degrading organic pollutants by constructing composites with Ag_2O. Nanomaterials. 2021;11:E1451.
13. Riazian M, Yousefpoor M. Photocatalytic activity, nanostructure and optical properties of 3D ZnS urchin-like via hydrothermal method. Int J Smart Nano Mater. 2020;11:47–64.

14. Chauhan R, Kumar A, Chaudhary RP. Photocatalytic degradation of methylene blue with Cu doped ZnS nanoparticles. J Lumin. 2014;145:6–12.
15. Ye Z, Kong L, Chen F, Chen Z, Lin Y, Liu C. A comparative study of photocatalytic activity of ZnS photocatalyst for degradation of various dyes. Optik. 2018;164:345–54.
16. Huo F, Wang Y, You C, Deng W, Yang F, Pu Y. Phase- and size-controllable synthesis with efficient photocatalytic activity of ZnS nanoparticles. J Mater Sci. 2017;52:5626–33.
17. Yin L, Wang D, Huang J, Cao L, Ouyang H, Yong X. Morphology-controllable synthesis and enhanced photocatalytic activity of ZnS nanoparticles. J Alloys Compd. 2016;664:476–80.
18. Bhatia S, Verma N. Photocatalytic activity of ZnO nanoparticles with optimization of defects. Mater Res Bull. 2017;95:468–76.
19. Wang M, Sun L, Fu X, Liao C, Yan C. Synthesis and optical properties of ZnS:Cu(II) nanoparticles. Solid State Commun. 2000;115:493–6.
20. Jothibas M, Manoharan C, Jeyakumar SJ, Praveen P, Punithavathy IK, Richard JP. Synthesis and enhanced photocatalytic property of Ni doped ZnS nanoparticles. Sol Energy. 2018;159:434–43.
21. Wang C, Hu B, Chen L, Liu N, Li J. Preparation and characterization of ZnS nanostructures. Optik. 2020;224:E165673.
22. Mishra P, Ojha KS, Khare A. Structural and optical study of copper-doped zinc sulfide nanoparticles. J Appl Spectrosc. 2018;85:743–8.
23. Tian ZM, Yuan SL, He JH, Li P, Zhang SQ, Wang CH, et al. Structure and magnetic properties in Mn doped SnO_2 nanoparticles synthesized by chemical co-precipitation method. J Alloys Compd. 2008;466:26–30.
24. Sathishkumar M, Saroja M, Venkatachalam M. Influence of (Cu, Al) doping concentration on the structural, optical and antimicrobial activity of ZnS thin films prepared by sol-gel dip coating techniques. Optik. 2019;182:774–85.
25. Chaliha C, Nath B, Verma P, Kalita E. Synthesis of functionalized Cu:ZnS nanosystems and its antibacterial potential. Arab J Chem. 2019;12:515–24.
26. Jasna VC, Anilkumar T, Ramesan MT. Nanocomposite materials based on zinc sulfide nanoparticles reinforced chlorinated styrene butadiene rubber. J Appl Polym Sci. 2018;135:E46538.
27. Alenad AM, Fatima S, Khalid U, Bano N, Abid AG, Manzoor S, et al. Polyaniline-engineered zinc sulphide nanocomposite as a highly efficient electrocatalyst for the oxygen evolution process. J Korean Ceram Soc. 2023;60:868–80.
28. Hosseini-Sarvari M, Sheikh H. Reduced graphene oxide–zinc sulfide (RGO–ZnS) nanocomposite: a new photocatalyst for oxidative cyclization of benzylamines to benzazoles under visible-light irradiation. React Chem Eng. 2022;7:2202–10.
29. Qin Y, Sun Z, Zhao W, Liu Z, Ni D, Ma Z. Improved photocatalytic properties of ZnS/RGO nanocomposites prepared with GO solution in degrading methyl orange. Nano-Struct Nano-Objects. 2017;10:176–81.
30. Dadi R, Azouani R, Traore M, Mielcarek C, Kanaev A. Antibacterial activity of ZnO and CuO nanoparticles against gram positive and gram negative strains. Mater Sci Eng C. 2019;104:E109968.
31. Khatoon UT, Velidandi A, Rao GVSN. Copper oxide nanoparticles: synthesis via chemical reduction, characterization, antibacterial activity, and possible mechanism involved. Inorg Chem Commun. 2023;149:E110372.
32. Cruz IF, Freire C, Araújo JP, Pereira C, Pereira AM. Multifunctional ferrite nanoparticles: from current trends toward the future. In: El-Gendy AA, Barandiarán JM, Hadimani RL, editors. Micro and nano technologies. Amsterdam: Elsevier; 2018. p. 59–116.
33. Thakur M, Kumar P, Thakur N, Kumar K, Jeet K, Kumar S, Thakur N. Photocatalytic, antibacterial and antioxidant potential of spheroidal shape chromium and yttrium doped cobalt oxide nanoparticles: a green approach. J Ind Chem Soc. 2024;101:E101199.
34. Kumar P, Thakur N, Kumar K, Kumar S, Dutt A, Thakur VK, Gutierrez-Rodelo C, Thakur P, Navarrete A, Thakur N. Catalyzing innovation: exploring iron oxide nanoparticles-Origins, advancements, and future application horizons. Coord Chem Rev. 2024;507:E215750.
35. Rana A, Kumar P, Thakur N, Kumar S, Kumar K, Thakur N. Investigation of photocatalytic, antibacterial and antioxidant properties of environmentally green synthesized zinc oxide and yttrium doped zinc oxide nanoparticles. Nano-Struc Nano-Objec. 2024;38:E101188.
36. Thakur N, Thakur N. Degradation of textiles dyes and scavenging activity of spherical shape obtained anatase phase of Co-Ni-doped TiO_2 nanocatalyst. J Mater Sci Mater Electon. 2024;35:E134.
37. Kumar P, Pathak D, Thakur N. Trimetallic doped hematite (α-FeO) nanoparticles using biomolecules of *Azadirachta indica* leaf extract for photocatalytic dye removal: insights into catalyst stability and reusability. Emerg Mater. 2024. https://doi.org/10.1007/s42247-24-00742-w.
38. Kumar P, Tapwal A, Kumar S, Thakur N. Improved photocatalytic and free radical scavenging studies of synthesized polymer PVP/*Azadirachta indica* leave extract-mediated Ni-Zn doped hematite nanoparticles. Adv Nat Sci Nanosci Nanotechnol. 2024;158:E025014.
39. Thakur N, Kumar P. Effect of shape and size on synthesized triple (Co/Ni/Zn) doped α-Fe_2O_3 nanoparticles on their photocatalytic and scavenging properties. Int J Nanosci. 2024. https://doi.org/10.1142/S0219581X24500108.
40. Umar K, Mfarrej MFB, Rahman KI, Zuhaib M, Khan A, Zia Q, Banawas S, Nadeem H, Khan MF, Ahmad F. ZnO nano-swirlings for azo dye AR183 photocatalytic degradation and antimycotic activity. Sci Rep. 2022;12:E14023.
41. Jethave G, Fegade U, Inamuddin, Altalhi T, Khan MF, Barhate B, Suryawanshi KE, Isai KA. Adsorption of congo red dye on CuO nanoparticles synthesized by green method using *Nyctanthes arbor*-tristis leaf extract: experimental and theoretical study. Int J Chem Kinet. 2022;54:513–22.
42. Khanr A, Mfarrej MFB, Khan MF, Khan S, Malan P, Saxena SC, Mudassir M, Ahmad F. Sea urchins like zinc oxide nanometric mitigating *Meloidogyne incognita* infection in eggplant. Cogent Food Agric. 2024;10:E2366396.
43. Al Baroot A, Alheshibri M, Drmosh QA, Akhtar S, Kotb E, Elsayed KA. A novel approach for fabrication ZnO/CuO nanocomposite via laser ablation in liquid and its antibacterial activity. Arab J Chem. 2022;15:E103606.
44. Mohammed R, Ali MEM, Gomaa E, Mohsen M. Copper sulfide and zinc oxide hybrid nanocomposite for wastewater decontamination of pharmaceuticals and pesticides. Sci Rep. 2022;12:E18153.
45. Yousefinia A, Khodadadi M, Mortazavi-Derazkola M. An efficient biosynthesis of novel ZnO/CuO nanocomposites using berberis vulgaris extract (ZnO/CuO@BVENCs) for enhanced photocatalytic degradation of pollution, antibacterial and antifungal activity. Environ Technol Innov. 2023;32:E103140.
46. Jayanetti M, Thambiliyagodage C, Liyanaarachchi H, Ekanayake G, Mendis A, Usgodaarachchi L. In vitro influence of PEG functionalized ZnO–CuO nanocomposites on bacterial growth. Sci Rep. 2024;14:E1293.
47. Hameed ASH, Karthikeyan C, Sasikumar S, Kumar VS, Kumaresan S, Ravi G. Impact of alkaline metal ions Mg^{2+}, Ca^{2+}, Sr^{2+} and Ba^{2+} on the structural, optical, thermal and antibacterial properties of ZnO nanoparticles prepared by the co-precipitation method. J Mater Chem B. 2013;1:5950–62.
48. Srivastava R, Pandey N, Mishra S. Effect of Cu concentration on the photoconductivity properties of ZnS nanoparticles synthesized by co-precipitation method. Mater Sci Semicond Proc. 2013;16:1659–64.
49. Alharbi A, Shah RK, Sayqal A, Subaihi A, Alluhaybi AA, Algethami FK, et al. Facile synthesis of novel zinc sulfide/chitosan composite for efficient photocatalytic degradation of acid brown 5G and acid black 2BNG dyes. Alex Eng J. 2020;60:2167–78.
50. Kuppayee M, Nachiyar GKV, Ramasamy V. Synthesis and characterization of Cu $^{2+}$ doped ZnS nanoparticles using TOPO and SHMP as capping agents. Appl Surf Sci. 2011;257:6779–86.
51. Aziz A, Ali N, Khan A, Bilal M, Malik S, Ali N, Khan H. Chitosan-zinc sulfide nanoparticles, characterization and their photocatalytic degradation efficiency for azo dyes. Int J Biol Macromol. 2020;153:502–12.
52. Alwany A, Alnakhlani A, Youssef G, Algradee M, Hassan B. Effect of Li+ concentration on the structural and optical properties of chemically synthesized ZnS nanoparticles. Results Opt. 2023;12:E100424.
53. Dhupar A, Kumar S, Tuli HS, Sharma AK, Sharma V, Sharma JK. In-doped ZnS nanoparticles: structural, morphological, optical and antibacterial properties. Appl Phys A. 2021;127:E263.
54. Riyas ZM, Prabhu MR, Sankaranarayanan K. Hydrothermal synthesis of La_2O_3–ZnO nanocomposites as electrode material for asymmetric supercapacitor applications. J Mater Sci Mater Electron. 2023;34:E1612.
55. Maheshwaran G, Seethalakshmi G, Devi VK, VenkataKrishna LM, Prabhu MR, Kumar MK, Sudhahar S. Synergistic effect of Cr_2O_3 and Co_3O_4 nanocomposite electrode for high performance supercapacitor applications. Curr Appl Phys. 2022;36:63–70.
56. Pegallapati P, Reddivari M, Pejjai B, Kummara T, Kotte T. Synthesis of Cu-doped ZnS nano-powder by chemical co-precipitation process. Mater Today Proc. 2023. https://doi.org/10.1016/j.matpr.2023.02.419.

57. Haritha V, Gowri S, Janarthanan B, Faiyazuddin M, Karthikeyan C, Sharmila S. Biogenic synthesis of nickel oxide nanoparticles using *Averrhoa bilimbi* and investigation of its antibacterial, antidiabetic and cytotoxic properties. Inorg Chem Commun. 2022;144:E109930.
58. Guhan V, Sanjana S, Gowri S, Karthikeyan C, Faiyazuddin M, Hirad AH, et al. Synergistic effect of coconut milk and water on synthesizing zinc oxide nanoparticles and its antibacterial properties. Biomass Convers Biorefin. 2023. https://doi.org/10.1007/s13399-023-04574-2.
59. Dwivedi P, Chauhan P, Tripathi D. Effect of Cu-doping and thermal treatment on antibacterial potential of ZnS nanoparticles. Mater Today Proc. 2022;62:6171–6.
60. Karthikeyan C, Sisubalan N, Sridevi M, Varaprasad K, Ghouse Basha M, Shucai W, Sadiku R. Biocidal chitosan-magnesium oxide nanoparticles via a green precipitation process. J Hazard Mater. 2021;411:E124884.
61. Choi S, Liu X, Pan Z. Zinc deficiency and cellular oxidative stress: prognostic implications in cardiovascular diseases. Acta Pharmacol Sin. 2018;39:1120–32.

Publisher's Note